Energy Storage Materials 24 (2020) 458–466

Contents lists available at ScienceDirect

Energy Storage Materials

journal homepage: www.elsevier.com/locate/ensm

New conversion chemistry of $CuSO_4$ as ultra-high-energy cathode material for rechargeable sodium battery

Yongseok Lee [a], Chang-Heum Jo [a], Jung-Keun Yoo [b], Ji Ung Choi [a], Wonseok Ko [a], Hyunyoung Park [a], Jae Hyeon Jo [a], Dong Ok Shin [c,d], Seung-Taek Myung [a,**], Jongsoon Kim [a,*]

[a] Department of Nanotechnology and Advanced Materials Engineering, Sejong University, Seoul, 05006, Republic of Korea
[b] Carbon Composites Department, Composites Research Division, Korea Institute of Materials Science (KIMS), 797 Changwondaero, Changwon, Republic of Korea
[c] Multidisciplinary Sensor Research Group, Electronics and Telecommunications Research Institute (ETRI), Daejeon, 305-700, Republic of Korea
[d] Department of Advanced Device Engineering, University of Science and Technology (UST), 217 Gajeongno, Yuseong-gu, Daejeon, 305-350, Republic of Korea

ARTICLE INFO

Keywords:
Cupric sulfate
High energy density
Cathode
Na-ion batteries

ABSTRACT

We report the nano-sized $CuSO_4$–carbon nanotube composite (nano-$CuSO_4$/C) as a novel conversion-based cathode material for Na-ion batteries (NIBs). The nano-$CuSO_4$/C undergoes a conversion reaction during the charge/discharge process with a high redox potential of ~2.7 V (*vs.* Na^+/Na) and the highest reported energy density for NIB cathode materials. Nano-$CuSO_4$/C exhibits excellent electrochemical performance, with a specific capacity of ~335 mAh g^{-1} at a rate of C/30 (1C = 335 mA g^{-1}), and even at 5C, its capacity is maintained up to ~204 mAh g^{-1}, corresponding to ~61% of the theoretical capacity. Furthermore, nano-$CuSO_4$/C delivers outstanding capacity retention of ~72% over 300 cycles at 2C with high coulombic efficiency of more than 99%. We confirm the reversible sodium storage mechanism on nano-$CuSO_4$/C under Na-ion battery system using various analyses, such as *operando/ex situ* X-ray diffraction, X-ray absorption near edge structure spectroscopy, extended X-ray absorption fine structure spectroscopy, transmission electron microscopy, and time-of-flight secondary-ion mass spectroscopy. $CuSO_4$ is transformed into Cu^0 and Na_2SO_4 during the discharge (reduction) process, and the original $CuSO_4$ is recovered during the charge (oxidation) process. This fundamental understanding of $CuSO_4$ provides insight for the use of high-capacity conversion-based cathode materials in NIBs.

1. Introduction

The use of fossil fuels contributes to environmental problems, such as the greenhouse effect and air pollution; thus, the development of eco-friendly electric vehicles (EVs) is needed [1–4]. To power EVs, Li-ion batteries (LIBs) have attracted great attention because of their high energy density and reasonable cycle life [5–7]. However, the extension of the application of LIBs from power sources for portable electronic devices to grid-scale applications has resulted in a shortage of lithium resources to satisfy the demands of various technologies and industries, thereby increasing the price of lithium [8–11]. The recent development of alternative battery systems with lower production cost than LIBs has led to the introduction of Na-ion batteries (NIBs) [12–15] because of the abundant Na resources in seawater and their similar reaction mechanisms as LIBs [16–18]. Over the last decade, there have been many works on intercalation-based cathode materials for NIBs [19–24]. The resulting energy densities depend on the crystal structures, such as whether the environment of sodium ions is octahedral [25] or prismatic [26] with an oxide [27] or polyanion [28] framework. Nevertheless, even though NIBs have advantages in terms of production cost, the energy densities of most reported intercalation-based cathodes for NIBs cannot compete with those for LIBs [29–37]. Moreover, if we rely on the same energy storage mechanisms for NIBs as those employed in LIBs, we will not be able to overcome this lower-energy-density issue.

Herein, we introduce a novel conversion-based cathode material with high redox potential. Compared with intercalation chemistry, which is the general mechanism used for sodium storage for cathode materials, the conversion reaction enables the storage of more sodium [38–41]. However, in general, conversion-based electrode materials exhibit lower redox potentials than intercalation-based electrode materials [42–44]. Thus, to date, the conversion reaction has been applied to the anode and not the cathode for LIBs and NIBs. Our strategy to increase the redox

* Corresponding author.
** Corresponding author.
E-mail addresses: smyung@sejong.ac.kr (S.-T. Myung), jongsoonkim@sejong.ac.kr (J. Kim).

https://doi.org/10.1016/j.ensm.2019.07.013
Received 15 March 2019; Received in revised form 16 April 2019; Accepted 10 July 2019
Available online 13 July 2019

potential is to maximize the inductive effect by using ions with high electronegativity. For the intercalation reaction, polyanion-based materials with P or S have higher operation voltages than normal transition-metal-oxide materials [45–48]; thus, we anticipate that a similar effect will be observed in conversion-based cathode materials with high redox potential through the inductive effect. Furthermore, it has been known that difference in Gibbs free energy for each conversion reaction determines the potential cell potential E^0 and the equation between Gibbs free energy and cell potential is as follows;

$$E^0 = -\frac{\Delta_r G^0}{zF} \quad (\Delta_r G^0 = \Delta_r H^0 - T\Delta_r S^0) \tag{1}$$

where $\triangle_r G^0$ is the difference of Gibbs free energy per mole between products and reactants at standard conditions, which is affected by the reaction enthalpy $\triangle_r H^0$; z is the number of moles of electrons transferred in the reaction; and F is the Faraday constant. Thus, for high operation voltage, electrode materials should have a large negative value of $\triangle_r G^0$. Cu-based compounds, such as oxide, sulfide and fluoride, have known to exhibit lower formation energies (or less negative value) than the compounds composed of other transition metal elements such as Fe, Mn and Co that are generally adopted as cathode materials for NIBs [49,50]. Table S1 presents standard Gibbs free energies/enthalpies of various transition metal compounds connected with different anions. These represent that Cu-based compounds can have higher redox potential than other metal-based compounds.

As a promising conversion-based cathode material for NIBs, we propose the nano-sized $CuSO_4$ – carbon nanotube composite (nano-$CuSO_4$/C) electrode with ultra-high energy density for the first time. The specific capacity delivered ~335 mAh g^{-1} with a high redox potential of ~2.7 V (*vs.* Na^+/Na) at C/30 (1C = 335 mA g^{-1}), resulting in the highest energy density of cathode materials for NIBs reported to date. Even at 5C, the nano-$CuSO_4$/C electrode delivered ~204 mAh g^{-1}, corresponding to ~61% of its theoretical capacity. Furthermore, over 300 cycles at 2C, charge/discharge capacities of the nano-$CuSO_4$/C electrode were maintained up to ~78% of the initial capacity with a high Coulombic efficiency (CE) of more than ~99%. The conversion reaction mechanism of $CuSO_4$ under Na-ion battery system was confirmed through the various analyses, such as *operando/ex situ* X-ray diffraction (XRD), X-ray absorption near edge structure spectroscopy (XANES), extended X-ray absorption fine structure spectroscopy (EXAFS), transmission electron microscopy (TEM) and time-of-flight secondary-ion mass spectroscopy (ToF-SIMS). The characterization results clearly indicate the occurrence of the following reversible conversion reaction of $CuSO_4$ during charge/discharge: $CuSO_4 + 2Na^+ + 2e^- \leftrightarrow Na_2SO_4 + Cu$.

2. Results and discussion

The preparation process and reaction mechanism for $CuSO_4$ are illustrated in Fig. 1 After dehydration of $CuSO_4{\cdot}5H_2O$ by heat treatment at 500 °C in air, the obtained $CuSO_4$ was intimately blended with conductive Super P carbon and multiwall carbon nanotubes using planetary ball milling to prepare a nano-sized nano-$CuSO_4$/C composite; this process enlarges the surface area, leading to a fast conversion reaction with Na ions. As shown in Fig. S1, it was verified through the thermogravimetric analysis (TGA) that ~20 wt% carbon contents exist in the nano-$CuSO_4$/C composite, which means that the nano-$CuSO_4$/C composite is composed of ~80 wt% $CuSO_4$ and ~20 wt% conductive carbons. It was hypothesized that the $CuSO_4$ is converted into metallic Cu^0 and Na_2SO_4 on discharge, and, during the charge process, these phases are reversibly recovered to $CuSO_4$, as indicated below:

$$CuSO_4 + 2Na^+ + 2e^- \leftrightarrow Cu + Na_2SO_4 \tag{2}$$

Using first-principles calculations, we predicted the theoretical redox potential for this reaction. The equation used to calculate the voltage profile of $CuSO_4$ during the conversion reaction is expressed as follows:

$$V = -\frac{E(Cu) + E(Na_2SO_4) - E(CuSO_4) - 2E(Na)}{2F} \tag{3}$$

where V is the average redox potential for the conversion reaction of $CuSO_4$, E is the formation energy of each component based on density functional theory (DFT), and F is the Faraday constant. The formation energies of each component are tabulated in Table S2. Despite the conversion reaction, it is surprising that the predicted redox potential of $CuSO_4$ is ~2.7 V (vs. Na^+/Na), which is the highest reported operation voltage among conversion-based electrode materials for NIBs to the best of our knowledge. The predicted theoretical capacity of $CuSO_4$ under the conversion reaction is ~335 mAh g^{-1}.

The crystal structure of nano-$CuSO_4$/C was verified using XRD with Rietveld refinement. As shown in Fig. 2, phase-pure nano-$CuSO_4$/C was synthesized, and its XRD pattern can be indexed to the *Pnma* space group. The calculated lattice parameters were $a = 8.3991(17)$ Å, $b = 6.6996(8)$ Å, $c = 4.8249(10)$ Å, and $\beta = 90°$, which are consistent with the previously reported values [51]. Fig. S2 compares the crystal structure and morphology of the as-prepared $CuSO_4$ and nano-$CuSO_4$/C, revealing a decrease in the particle size but no change in the crystal structure. Moreover, we calculated the crystallite size of $CuSO_4$ phase in the nano-$CuSO_4$/C composite using Scherrer equation (Table S3). It was verified that the average crystallite size of $CuSO_4$ phase is ~14.51 nm, which indicates that the $CuSO_4$ nanocrystals were well prepared through the high-energy ball-milling process. This modification is likely to improve the interfacial reaction kinetics via the shortened diffusion path [52–54]. In addition, it was reported that the long ion diffusion length and large band-gap of the conversion-based electrode materials result in their poor ionic/electronic conductivity, which is considered as the major drawbacks that prevent the implementation of the theoretical capacity of the conversion-based electrode materials [50,55]. Interestingly, it was verified through the electrochemical tests that the nano-$CuSO_4$/C composite delivered the theoretical capacity of $CuSO_4$ at the mild condition. We supposed that the nano-sizing and the carbon-mixing using high-energy ball milling enable the implementation of the theoretical capacity of $CuSO_4$. The nano-sizing of $CuSO_4$ through high-energy ball-milling can provide shorten ion diffusion path. The diffusion time (τ) can be represented as the following equation:

$$\tau = L_{Na}^2 / D_{Na} \tag{4}$$

where L_{Na} is the diffusion length of Na ions and D_{Na} is the diffusion coefficient of Na ions. According to the equation, the diffusion time is decreased as square of diffusion length, which indicates that shortened diffusion length can result in the facile Na ionic diffusion and the significantly improved electrochemical performance of $CuSO_4$. Moreover, the homogeneous carbon-mixing of $CuSO_4$ through high-energy ball-milling can significantly improve the electronic conductivity of $CuSO_4$, thus, it can enhance the electrochemical performances of active material via effective diffusion of not only e^- but also Na^+. In addition, poor electrochemical performances of the pristine $CuSO_4$ electrode indicates that without the nano-sizing and the carbon-mixing using high-energy ball milling, it is difficult at the mild condition to implement the theoretical capacity of $CuSO_4$.

To confirm the predicted high redox potential of $CuSO_4$, we measured the electrochemical performances of the nano-$CuSO_4$/C composite electrode in Na cells. Fig. 3a shows that the nano-$CuSO_4$/C exhibited the average operation voltage of ~2.7 V (*vs.* Na^+/Na), which is higher than the other conversion-based electrode for NIBs. The specific capacities of the nano-$CuSO_4$/C composite measured under different currents ranging from C/30 to 5C (1C = ~335 mAh g^{-1}) indicate that the nano-$CuSO_4$/C composite delivered acceptable power for a NIB (Fig. 3b). The specific discharge capacity of the nano-$CuSO_4$/C composite at C/30 was comparable to the theoretical capacity of $CuSO_4$ (~335 mAh g^{-1} with two-electron transfer as indicated in Eq. (2)). It is surprising that even at 5C, its discharge/charge capacities were maintained up to ~204 mAh g^{-1} with a high CE of over 99%. We also measured the electrochemical

properties of pristine $CuSO_4$ without nano-sizing (Fig. S3). Even though the mass ratio of $CuSO_4$, carbon and binder contents in the pristine $CuSO_4$ electrode were same as that in the nano-$CuSO_4$/C electrode, Unlike the nano-$CuSO_4$/C composite, the pristine $CuSO_4$ delivered poor specific capacities even at the low current rate of C/30, which indicates the importance of nano-sizing and conductive carbon matrix to enhance the electrochemical performances of $CuSO_4$. Furthermore, over 300 cycles measured at 2C, the nano-$CuSO_4$/C composite delivered the capacity retention of ~78% compared to its initial capacity and the CE was more than 99% (Fig. 3c and Fig. S4). These results indicate the outstanding cyclability of the nano-$CuSO_4$/C composite as the promising cathode for NIBs. The capacities calculated at the basis of the scale of the nano-$CuSO_4$/C composite are shown in Fig. S5. Moreover, to verify the capacity contribution of ball-milled carbons, we prepared the nano-$ZnSO_4$/C composite. All preparation processes of the nano-$ZnSO_4$/C composite were same as those of the nano-$CuSO_4$/C composite, such as the 20 wt% carbon contents and the high-energy ball-milling processes. As shown in Fig. S6, unlike the nano-$CuSO_4$/C electrode, the nano-$ZnSO_4$/C electrode exhibited poor electrochemical performances, which indicates that the capacity contribution of ball-milled carbons in the nano-$CuSO_4$/C composite is negligible. In addition, it was verified that, after 300 cycles, any cracks or structural deformation was hardly observed in the nano-$CuSO_4$/C electrode (Fig. S7). As shown in Fig. S8, we performed a full cell test using nano-$CuSO_4$/C with pre-sodiated hard carbon electrodes for 50 cycles at 1C within the voltage range between 1.1 V and 4.0 V. The fabricated full cell was able to exhibit moderate performances for 50 cycles with ~90% retention of initial capacity, which implies that the present nano-$CuSO_4$/C can be applicable to the cathode for NIBs.

The structural evolution of the $CuSO_4$ composite electrode was monitored using *operando* XRD at the first cycle. The full *operando* XRD patterns were presented in Fig. S9. As shown in Fig. 4a, a new peak appeared at ~43.4° (2θ), which corresponds to the (111) peak of Cu metal on discharge (reduction) to 1.2 V, and the original $CuSO_4$ phase became less evident as sodiation progressed. This evolution results from the conversion process in which $CuSO_4$ was rearranged via decomposition and formation of metallic Cu^0. No other peaks were obvious in the *operando* XRD pattern (Fig. 4a) other than the two phases at ~32.5° (2θ) (Na_2SO_4) and ~43.4° (2θ) (metallic Cu^0). This finding agrees with our hypothesis expressed by reaction (2) that the $CuSO_4$ is fully converted via the predicted conversion reaction. On charge (oxidation), the relative intensities of the metallic Cu^0 and Na_2SO_4 phases were gradually diminished, and the $CuSO_4$ phase was somehow restored with low crystallinity via rearrangement of the crystal structure at the end of discharge. An additional finding was the appearance of new peaks at 22°–26° (2θ), which is attributed to the formation of Na_2SO_4. (Fig. S10). This result validates our hypothesis that the present $CuSO_4$ undergoes a reversible conversion reaction. The relative intensity of the XRD pattern for the recovered $CuSO_4$ was not much higher than that of the fresh electrode, which is associated with the formation of amorphous or low-crystalline nanosized $CuSO_4$. ToF-SIMS was employed to obtain further insight into the reaction process of $CuSO_4$ during the conversion process (Fig. 4b). For the fresh state, there was no indication of a Na^+ (m = 22.98) fragment; however, the presence of the $CuSO_3^+$ (m = 142.88) fragment indicated that the resulting compound was composed of Cu–S–O bonds. At the end of discharge, the strong signal of the $CuSO_3^+$ fragment was no longer observed, whereas Na^+ and $NaSO_2^-$ (m = 86.95) fragments appeared. This result indicates that there was no Cu–S–O bonding in the discharged (reduced) products. The presence of $NaSO_2^-$ supports the idea that the starting $CuSO_4$ was reorganized into Cu and Na_2SO_4 via reaction (2). After charge (oxidation) to 3 V, it is worth highlighting that the $CuSO_3^+$ fragment, observed in the fresh states, was observed again but that the $NaSO_2^-$ fragment was negligible. The presence of $CuSO_3^+$ fragment is indicative of a reversible conversion reaction, which restores the original $CuSO_4$ despite the low crystallinity resulting from the reorganization of the crystal structure by the electrochemical reaction.

The reaction mechanism of the conversion reaction of $CuSO_4$ in a Na cell was also identified using XANES and EXAFS analyses. As shown in Fig. 4c, during initial charging/discharging, the clear variations in the oxidation states of Cu^{2+} and metallic Cu^0 were verified. Furthermore, the simultaneous dissociation of the Cu–O bond and the formation of the metallic Cu–Cu bond during initial discharging was also confirmed by the Fourier transform (FT) of the EXAFS spectra. We also observed that the re-charging process of the electrode resulted in re-formation of the Cu–O

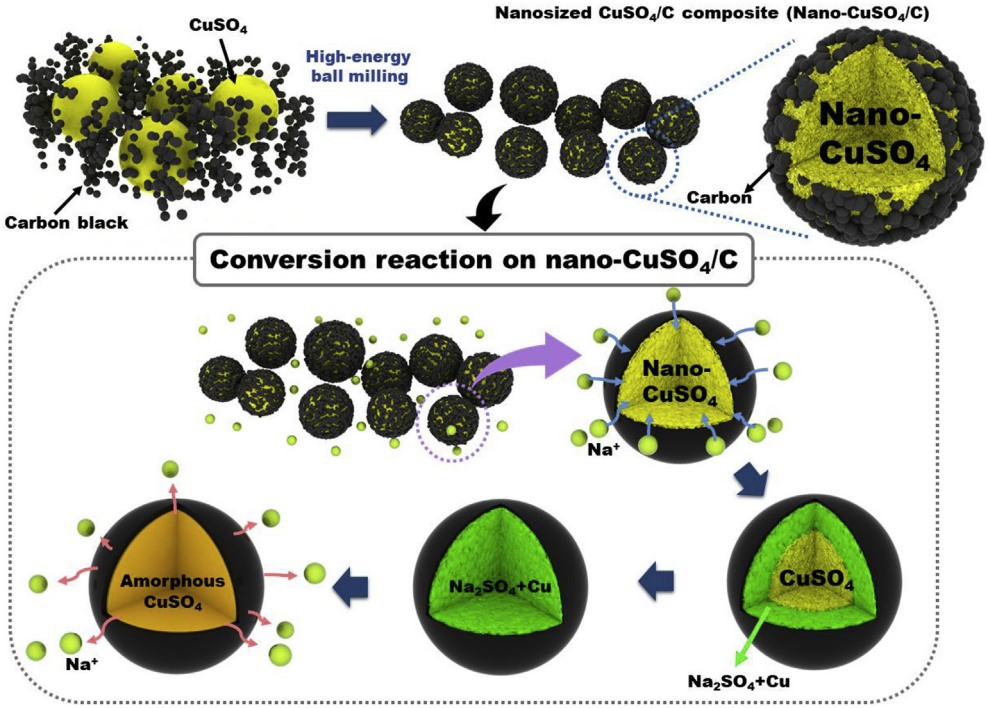

Fig. 1. Scheme of conversion reaction mechanism of nano-$CuSO_4$/C during charge/discharge process.

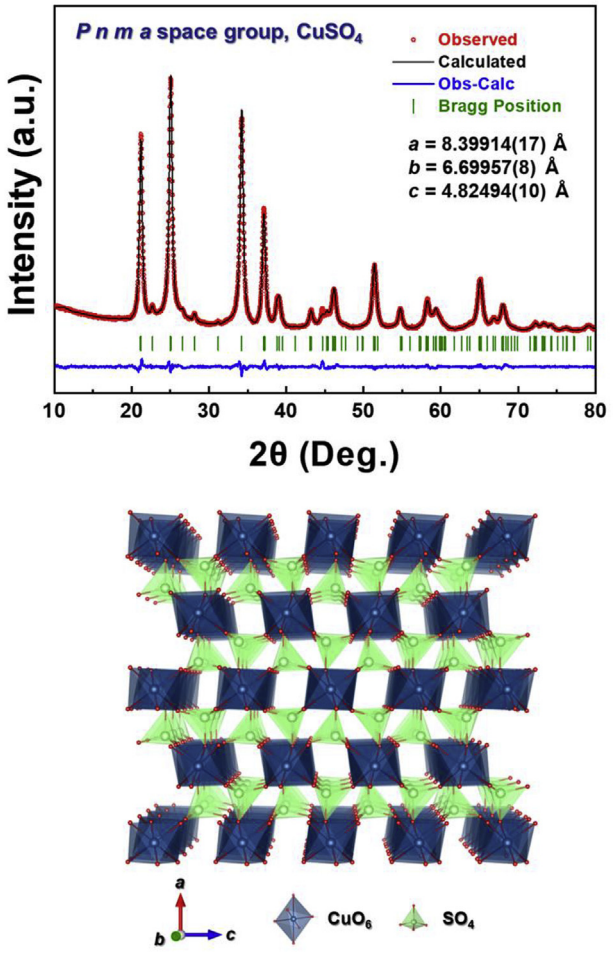

Fig. 2. Rietveld refinement of XRD pattern and crystal structure of nano-$CuSO_4$/C composite. ($R_P = 2.24\%$, $R_I = 1.72\%$, $R_F = 1.65\%$, and $\chi^2 = 1.88\%$).

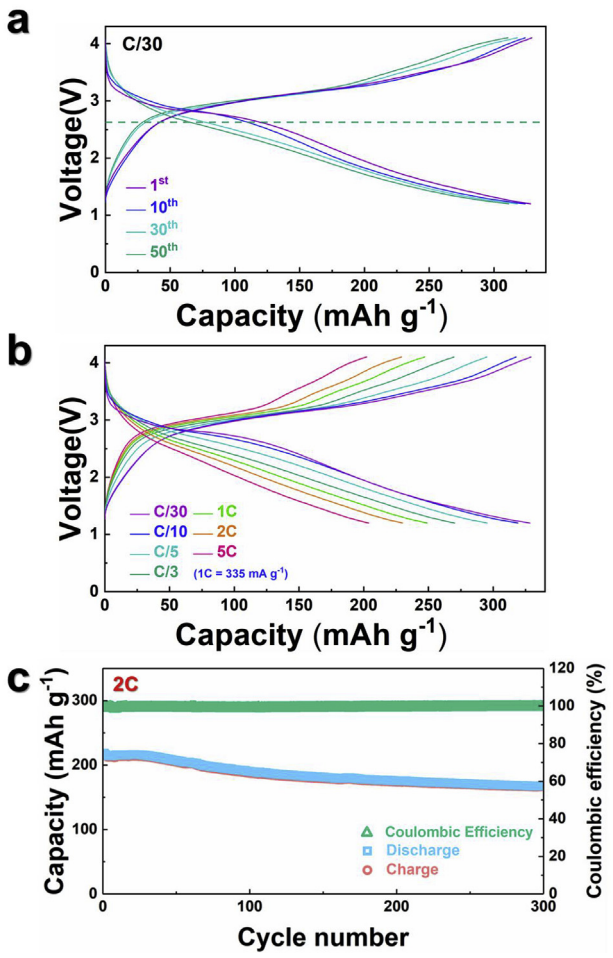

Fig. 3. (a) Charge–discharge curves of nano-$CuSO_4$/C obtained at a rate of C/30 (11.2 mA g^{-1}) at 1st, 10th, 30th and 50th cycles, which is compared to the theoretically predicted average operation voltage in the voltage range of 1.2–4.1 V (vs. Na^+/Na). (b) Power capability of nano-$CuSO_4$/C at various C-rates. (c) Cyclic performance and Coulombic efficiency of nano-$CuSO_4$/C over 300 cycles at 2C after 1 cycle at C/3.

bond with disappearance of the Cu–Cu bond (Fig. 4c). TEM with selected-area electron diffraction (SAED) analysis also revealed the overall conversion reaction of $CuSO_4$. As shown in Fig. 5a, the nano-$CuSO_4$/C composite was composed of small $CuSO_4$ nanocrystals (<10 nm) with interplanar crystal spacings of 0.42 and 0.26 nm, corresponding to the (101) and (121) planes of $CuSO_4$, respectively. During discharging, there were appearance of new nanocrystals with the crystal spacing of Na_2SO_4 and Cu metal but not for the existing $CuSO_4$ nanocrystals (Fig. 5b). Interestingly, $CuSO_4$ nanocrystals were reformed during charging (Fig. 5c), which is consistent with the XRD, ToF-SIMS, XANES, and EXAFS data shown in Fig. 4.

The idea behind the current work is to increase the redox potential using the induction effect of polyanions. As designed, the theoretical calculations and experiments demonstrated that the present nano-$CuSO_4$/C composite electrode exhibited an average operation voltage approximately 2.7 V vs. Na^+/Na and underwent a reversible conversion reaction by forming Na_2SO_4 as a conversion byproduct on reduction with subsequent oxidation restoring the original structure though showing low crystallinity. Through this reaction, the delivered capacity was retained for long-term cycling (~72% for 300 cycles), and the electrode performances were comparable or exceeded those of intercalation cathode materials for NIBs. Here, we present the conversion chemistry based on S–O bonding, and extension of the induction effect using different types of polyanions will be applied in future work to develop new conversion cathode materials that can provide high redox potential. We compared the electrochemical performances of cathode materials for NIBs reported to date (Fig. 6a), clearly presenting the outstanding properties of the nano-$CuSO_4$/C composite. In particular, we compared the power-capability, energy density, average potential of discharge, and cyclability of the nano-$CuSO_4$/C with those of the cathode materials with high specific capacity of more than 180 mAh g^{-1} (Fig. 6b and Table S4) [30,36,37,56–64], which highlights outstanding electrochemical performances of the present nano-$CuSO_4$/C as the promising cathode for NIBs.

3. Conclusions

We propose a new conversion-based cathode material, nano-$CuSO_4$/C composite, with a high energy density (specific capacity of 335 mAh g^{-1} with an average redox potential of ~2.7 V (*vs.* Na^+/Na)) and acceptable long-term cycling performance among reported cathode materials for NIBs. Unlike general conversion-based electrode materials, the nano-$CuSO_4$/C composite exhibits the high average operation voltage derived from the induction effect, which is verified by combined studies using first-principles calculations and experiments: $CuSO_4 + 2Na^+ + 2e^- \leftrightarrow Cu + Na_2SO_4$. We believe that our concept, which relies on the polyanion-induced high redox potential, will provide significant insight for the development of high-energy cathode materials for NIBs.

4. Experimental

4.1. Material preparation

The crystalline $CuSO_4$ powders were prepared by heating $CuSO_4$*5 H_2O (Sigma Aldrich, 98%) at 500 °C for 5 h in air. After dehydration, the powders were whitish-gray. The $CuSO_4$ was mixed with carbon using high-energy ball milling of 80 wt% $CuSO_4$ and 20 wt% Super P carbon black. The powders were placed into a nitride jar with thirty balls and ball milled at 500 rpm for 15 h.

4.2. Material characterization

The coated powders were characterized using XRD (PANalytical)

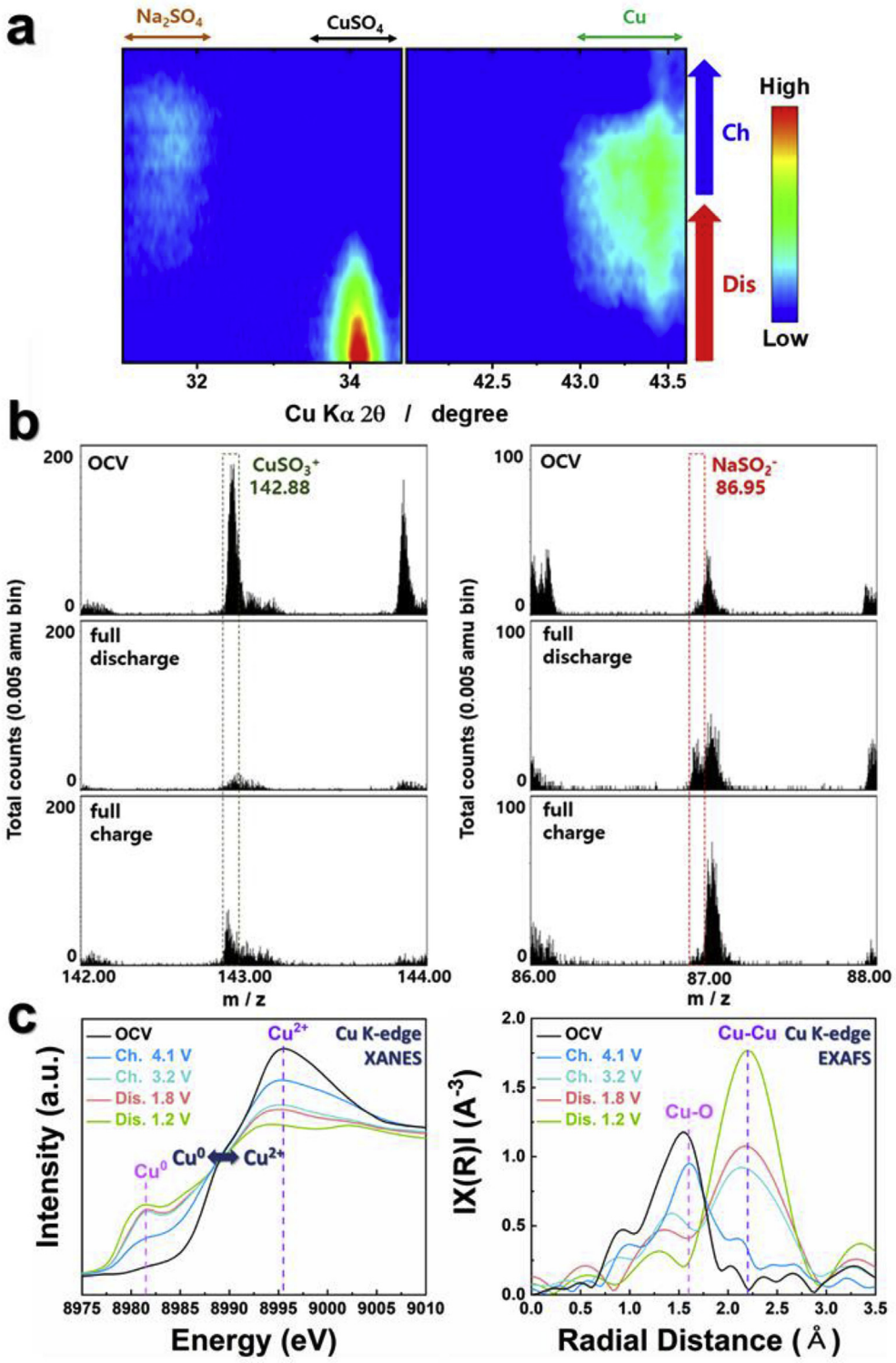

Fig. 4. (a) *Operando* XRD patterns of nano-$CuSO_4$/C electrode during the first cycle. (b) ToF-SIMS graphs of nano-$CuSO_4$/C samples during charge and discharge. (c) Cu K-edge XANES and EXAFS spectra of nano-$CuSO_4$/C samples.

using Cu Kα radiation (wavelength = 1.54178 Å). The 2θ range was 10°–60° with a time per step of 0.13. The FullProf Rietveld program was used to analyze the measured XRD data. The morphology of the materials was examined using SEM (SU-8010) and FESEM (JEM-2100F). XANES spectroscopy was performed on beamline 8D at the 3.0-GeV Pohang Light Source.

4.3. Electrochemical properties

The electrodes were fabricated from a slurry of 87.5 wt% nano-$CuSO_4$/C composite, 2.5 wt% Super-P carbon, and 10 wt% polyvinylidene fluoride (PVDF) binder in *N*-methyl-2-pyrrolidone (NMP), which indicates that the nano-$CuSO_4$/C electrode consisted of 70 wt%

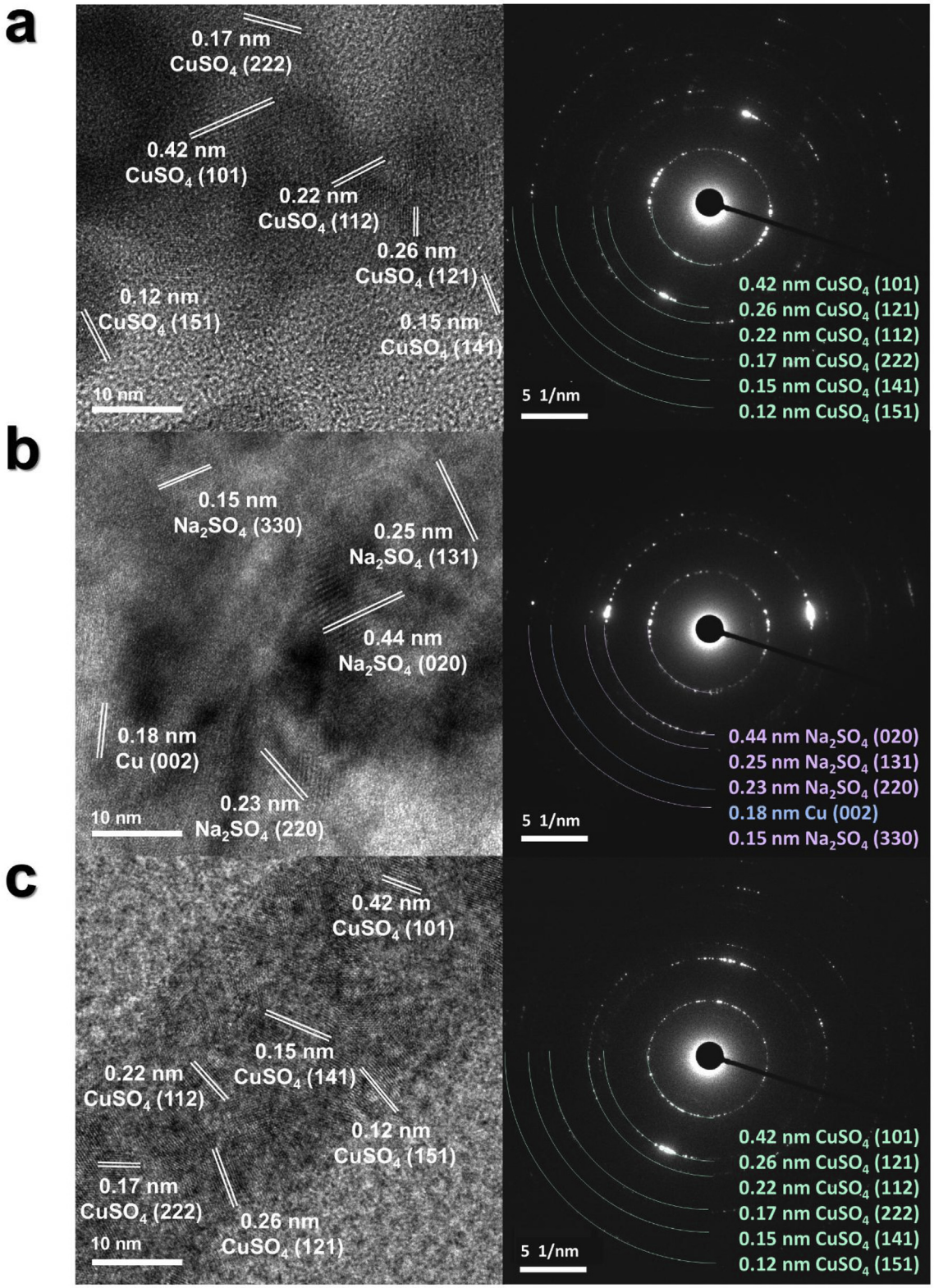

Fig. 5. HRTEM images and SAED patterns of (a) OCV, (b) discharged, (c) charged nano-$CuSO_4$/C composite.

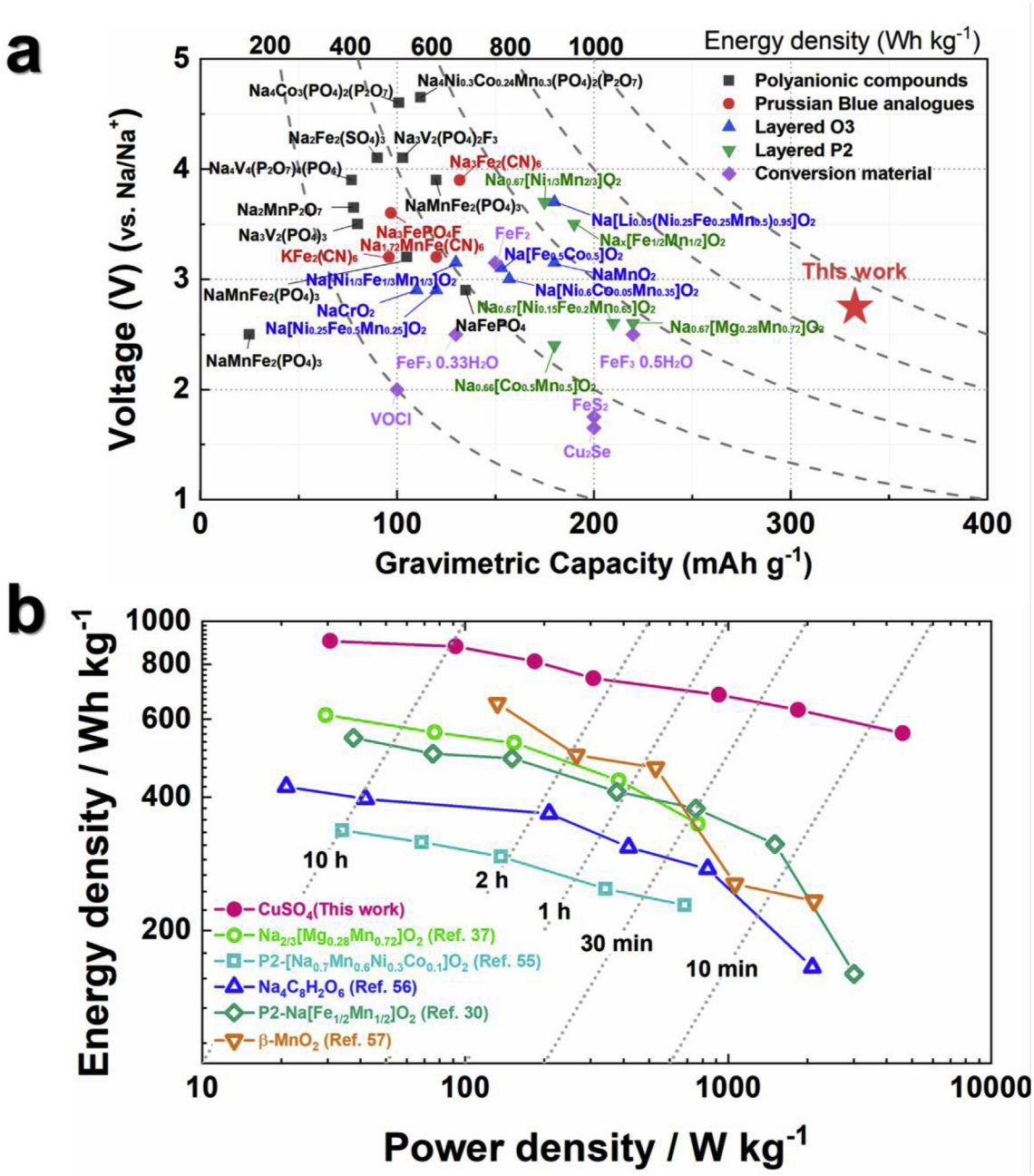

Fig. 6. (a) Comparison of electrochemical performances among the cathode materials for NIBs up to now. (b) Comparison of Ragone plot on the nano-$CuSO_4$/C and reported cathode materials with high specific capacity (>180 mAh g^{-1}).

$CuSO_4$ as the active material, 20 wt% conductive carbons and 10 wt% PVDF binder. For fair comparison of electrochemical performances between the nano-$CuSO_4$/C electrode and the pristine $CuSO_4$ electrode, we applied the same mass ratio of 70 wt% $CuSO_4$, 20 wt% conductive carbons and 10 wt% PVDF binder for preparation of s the nano-$CuSO_4$/C electrode and the pristine $CuSO_4$ electrode. The slurry was applied on Al foil using a doctor blade and dried in an oven for 12 h. R2032 cells were assembled in an argon-filled glove box using the $CuSO_4$ composite electrode, a Na counter electrode, a glass fiber separator, and 1 M $NaPF_6$ in EC:DMC:FEC (49:49:2 v/v%) as the electrolyte. The electrochemical performances of the cells were measured by charging and discharging in the voltage range of 1.2–4.1 V at 30 °C.

4.4. Computational details

Density functional theory (DFT) calculations were performed using the Vienna Ab initio Simulation Package (VASP) [65]. We used projector-augmented wave (PAW) pseudo potentials [66] with a plane-wave basis set, as implemented in VASP. Perdew–Burke–Ernzerhof (PBE) parametrization of the generalized gradient approximation (GGA) was used for the exchange-correlation function [67,68]. All the calculations were performed with an energy cutoff of 520 eV until the remaining force in the system converged to less than 0.05 eV $Å^{-1}$ per unit cell. The detailed parameters reported at the Materials Project [69], such as U values and energy-cutoff *etc.*, were used for this DFT calculation.

Conflicts of interest

There are no conflicts to declare.

Acknowledgements

This research was supported by the International Research & Development Program of the National Research Foundation of Korea funded by the Ministry of Science and ICT of Korea (NRF-2018K2A9A2A12000230), the National Research Foundation of Korea funded by the Ministry of Science & ICT (2017M2A2A6A01070834 (Radiation Technology R&D program), by an Institute for Information & communications Technology Promotion grant funded by the Korean government (MSIT) (No. 2017-0-00044, Development of Shape/Function-Controllable ICT Convergent Materials/Components for Next-Generation Mobilities), and supported by the Basic Science Research Program through the National Research Foundation, funded by the Ministry of Science and ICT of Korea (NRF-2015M3D1A1069713)).

Appendix A. Supplementary data

Supplementary data to this article can be found online at https://doi.org/10.1016/j.ensm.2019.07.013.

References

[1] M.D. Slater, D. Kim, E. Lee, C.S. Johnson, Sodium-ion batteries, Adv. Funct. Mater. 23 (2013) 947–958. https://doi.org/10.1002/adfm.201200691.
[2] V. Palomares, M. Casas-Cabanas, E. Castillo-Martinez, M.H. Han, T. Rojo, Update on Na-based battery materials. A growing research path, Energy Environ. Sci. 6 (2013) 2312–2337. https://doi.org/10.1039/c3ee41031e.
[3] D. Larcher, J.M. Tarascon, Towards greener and more sustainable batteries for electrical energy storage, Nat. Chem. 7 (2015) 19–29. https://doi.org/10.1038/nchem.2085.
[4] B. Dunn, H. Kamath, J.M. Tarascon, Electrical energy storage for the grid: a battery of choices, Science 334 (2011) 928–935. https://doi.org/10.1126/science.1212741.
[5] M. Armand, J.M. Tarascon, Building better batteries, Nature 451 (2008) 652–657. https://doi.org/10.1038/451652a.
[6] J.M. Tarascon, M. Armand, Issues and challenges facing rechargeable lithium batteries, Nature 414 (2001) 359–367. https://doi.org/10.1038/35104644.
[7] J.M. Zheng, M.H. Engelhard, D.H. Mei, S.H. Jiao, B.J. Polzin, J.G. Zhang, W. Xu, Electrolyte additive enabled fast charging and stable cycling lithium metal batteries, Nat. Energy 2 (2017) 8. https://doi.org/10.1038/nenergy.2017.12.
[8] P.W. Gruber, P.A. Medina, G.A. Keoleian, S.E. Kesler, M.P. Everson, T.J. Wallington, Global lithium availability a constraint for electric vehicles? J. Ind. Ecol. 15 (2011) 760–775. https://doi.org/10.1111/j.1530-9290.2011.00359.x.
[9] H. Vikstrom, S. Davidsson, M. Hook, Lithium availability and future production outlooks, Appl. Energy 110 (2013) 252–266. https://doi.org/10.1016/j.apenergy.2013.04.005.
[10] M.J. Choi, J. Kim, J.K. Yoo, S. Yim, J. Jeon, Y.S. Jung, Extremely small pyrrhotite Fe7S8 nanocrystals with simultaneous carbon-encapsulation for high-performance Na-ion batteries, Small 14 (2018) 6. https://doi.org/10.1002/smll.201702816.
[11] H. Kim, G. Yoon, I. Park, K.Y. Park, B. Lee, J. Kim, Y.U. Park, S.K. Jung, H.D. Lim, D. Ahn, S. Lee, K. Kang, Anomalous Jahn-Teller behavior in a manganese-based mixed-phosphate cathode for sodium ion batteries, Energy Environ. Sci. 8 (2015) 3325–3335. https://doi.org/10.1039/c5ee01876e.
[12] P.G. Bruce, B. Scrosati, J.M. Tarascon, Nanomaterials for rechargeable lithium batteries, Angew. Chem. Int. Ed. 47 (2008) 2930–2946. https://doi.org/10.1002/anie.200702505.
[13] S. Praneetha, A.V. Murugan, Development of sustainable rapid microwave assisted process for extracting nanoporous Si from earth abundant agricultural residues and their carbon-based nanohybrids for lithium energy storage, Acs. Sustain. Chem. Eng. 3 (2015) 224–236. https://doi.org/10.1021/sc500735a.
[14] H. Wu, Y. Cui, Designing nanostructured Si anodes for high energy lithium ion batteries, Nano Today 7 (2012) 414–429. https://doi.org/10.1016/j.nantod.2012.08.004.
[15] J. Kim, G. Yoon, M.H. Lee, H. Kim, S. Lee, K. Kang, New 4V-class and zero-strain cathode material for Na-ion batteries, Chem. Mater. 29 (2017) 7826–7832. https://doi.org/10.1021/acs.chemmater.7b02477.
[16] S.P. Ong, V.L. Chevrier, G. Hautier, A. Jain, C. Moore, S. Kim, X.H. Ma, G. Ceder, Voltage, stability and diffusion barrier differences between sodium-ion and lithium-ion intercalation materials, Energy Environ. Sci. 4 (2011) 3680–3688. https://doi.org/10.1039/c1ee01782a.
[17] L. Wang, Y.H. Lu, J. Liu, M.W. Xu, J.G. Cheng, D.W. Zhang, J.B. Goodenough, A superior low-cost cathode for a Na-ion battery, Angew. Chem. Int. Ed. 52 (2013) 1964–1967. https://doi.org/10.1002/anie.201206854.
[18] Y. Yamada, T. Doi, I. Tanaka, S. Okada, J. Yamaki, Liquid-phase synthesis of highly dispersed NaFeF3 particles and their electrochemical properties for sodium-ion batteries, J. Power Sources 196 (2011) 4837–4841. https://doi.org/10.1016/j.jpowsour.2011.01.060.
[19] R.A. Shakoor, D.H. Seo, H. Kim, Y.U. Park, J. Kim, S.W. Kim, H. Gwon, S. Lee, K. Kang, A combined first principles and experimental study on $Na_3V_2(PO_4)_2F_3$ for rechargeable Na batteries, J. Mater. Chem. 22 (2012) 20535–20541. https://doi.org/10.1039/c2jm33862a.
[20] J. Kim, D.H. Seo, H. Kim, I. Park, J.K. Yoo, S.K. Jung, Y.U. Park, W.A. Goddard, K. Kang, Unexpected discovery of low-cost maricite NaFePO4 as a high-performance electrode for Na-ion batteries, Energy Environ. Sci. 8 (2015) 540–545. https://doi.org/10.1039/c4ee03215b.
[21] Z.L. Jian, C.C. Yuan, W.Z. Han, X. Lu, L. Gu, X.K. Xi, Y.S. Hu, H. Li, W. Chen, D.F. Chen, Y. Ikuhara, L.Q. Chen, Atomic structure and kinetics of NASICON NaxV2(PO4)(3) cathode for sodium-ion batteries, Adv. Funct. Mater. 24 (2014) 4265–4272. https://doi.org/10.1002/adfm.201400173.
[22] M. Casas-Cabanas, V.V. Roddatis, D. Saurel, P. Kubiak, J. Carretero-Gonzalez, V. Palomares, P. Serras, T. Rojo, Crystal chemistry of Na insertion/deinsertion in $FePO_4$-$NaFePO_4$, J. Mater. Chem. 22 (2012) 17421–17423. https://doi.org/10.1039/c2jm33639a.
[23] Y.B. Shen, S. Birgisson, B.B. Iversen, A P2-$Na_xCo_{0.7}Mn_{0.3}O_2$ (x approximate to 1.0) cathode material for Na-ion batteries with superior rate and cycle capability, J. Mater. Chem. A 4 (2016) 12281–12288. https://doi.org/10.1039/c6ta03630a.
[24] C. Delacourt, P. Poizot, J.M. Tarascon, C. Masquelier, The existence of a temperature-driven solid solution in Li_xFePO_4 for $0 \leq x \leq 1$, Nat. Mater. 4 (2005) 254–260. https://doi.org/10.1038/nmat1335.
[25] J.Y. Hwang, S.T. Myung, Y.K. Sun, Sodium-ion batteries: present and future, Chem. Soc. Rev. 46 (2017) 3529–3614. https://doi.org/10.1039/c6cs00776g.
[26] Z.F. Dai, U. Mani, H.T. Tan, Q.Y. Yan, Advanced cathode materials for sodium-ion batteries: what determines our choices? Small Methods 1 (2017) 26. https://doi.org/10.1002/smtd.201700098.
[27] H. Su, S. Jaffer, H.J. Yu, Transition metal oxides for sodium-ion batteries, Energy Storage Materials 5 (2016) 116–131. https://doi.org/10.1016/j.ensm.2016.06.005.
[28] Q. Ni, Y. Bai, F. Wu, C. Wu, Polyanion-Type electrode materials for sodium-ion batteries, Adv. Sci. 4 (2017) 24. https://doi.org/10.1002/advs.201600275.
[29] R.M. Qiao, K.H. Dai, J. Mao, T.C. Weng, D. Sokaras, D. Nordlund, X.Y. Song, V.S. Battaglia, Z. Hussain, G. Liu, W.L. Yang, Revealing and suppressing surface Mn(II) formation of Na0.44MnO2 electrodes for Na-ion batteries, Nano Energy 16 (2015) 186–195. https://doi.org/10.1016/j.nanoen.2015.06.024.
[30] N. Yabuuchi, M. Kajiyama, J. Iwatate, H. Nishikawa, S. Hitomi, R. Okuyama, R. Usui, Y. Yamada, S. Komaba, P2-type $Na_x[Fe_{1/2}Mn_{1/2}]O_2$ made from earth-abundant elements for rechargeable Na batteries, Nat. Mater. 11 (2012) 512–517. https://doi.org/10.1038/nmat3309.
[31] M. Nose, H. Nakayama, K. Nobuhara, H. Yamaguchi, S. Nakanishi, H. Iba, Na4Co3(PO4)(2)P2O7: a novel storage material for sodium-ion batteries, J. Power Sources 234 (2013) 175–179. https://doi.org/10.1016/j.jpowsour.2013.01.162.
[32] H. Kim, R.A. Shakoor, C. Park, S.Y. Lim, J.S. Kim, Y.N. Jo, W. Cho, K. Miyasaka, R. Kahraman, Y. Jung, J.W. Choi, $Na_2FeP_2O_7$ as a promising iron-based pyrophosphate cathode for sodium rechargeable batteries: a combined experimental and theoretical study, Adv. Funct. Mater. 23 (2013) 1147–1155. https://doi.org/10.1002/adfm.201201589.
[33] J.Y. Hwang, S.T. Myung, C.S. Yoon, S.S. Kim, D. Aurbach, Y.K. Sun, Novel cathode materials for Na-ion batteries composed of spoke-like nanorods of Na $[Ni_{0.61}Co_{0.12}Mn_{0.27}]O_2$ assembled in spherical secondary particles, Adv. Funct. Mater. 26 (2016) 8083–8093. https://doi.org/10.1002/adfm.201603439.
[34] J.Y. Hwang, S.T. Myung, D. Aurbach, Y.K. Sun, Effect of nickel and iron on structural and electrochemical properties of O3 type layer cathode materials for sodium-ion batteries, J. Power Sources 324 (2016) 106–112. https://doi.org/10.1016/j.jpowsour.2016.05.064.
[35] X.H. Zhang, W.L. Pang, F. Wan, J.Z. Guo, H.Y. Lu, J.Y. Li, Y.M. Xing, J.P. Zhang, X.L. Wu, P2-$Na_{2/3}Ni_{1/3}Mn_{5/9}Al_{1/9}O_2$ microparticles as superior cathode material for sodium-ion batteries: enhanced properties and mechanisam via graphene connection, Acs. Appl. Mater. Inter. 8 (2016) 20650–20659. https://doi.org/10.1021/acsami.6b03944.
[36] G. Singh, J.M.L. del Amo, M. Galceran, S. Perez-Villar, T. Rojo, Structural evolution during sodium deintercalation/intercalation in $Na_{2/3}[Fe_{1/2}Mn_{1/2}]O_2$, J. Mater. Chem. A 3 (2015) 6954–6961. https://doi.org/10.1039/c4ta06360k.
[37] N. Yabuuchi, R. Hara, K. Kubota, J. Paulsen, S. Kumakura, S. Komaba, A new electrode material for rechargeable sodium batteries: P2-type $Na_{2/3}[Mg_{0.28}Mn_{0.72}]O_2$ with anomalously high reversible capacity, J. Mater. Chem. A 2 (2014) 16851–16855. https://doi.org/10.1039/c4ta04351k.
[38] R.J. Chen, R. Luo, Y.X. Huang, F. Wu, L. Li, Advanced high energy density secondary batteries with multi-electron reaction materials, Adv. Sci. 3 (2016) 39. https://doi.org/10.1002/advs.201600051.
[39] A. Kraytsberg, Y. Ein-Eli, A critical review-promises and barriers of conversion electrodes for Li-ion batteries, J. Solid State Electrochem. 21 (2017) 1907–1923. https://doi.org/10.1007/s10008-017-3580-9.
[40] F. Klein, B. Jache, A. Bhide, P. Adelhelm, Conversion reactions for sodium-ion batteries, Phys. Chem. Chem. Phys. 15 (2013) 15876–15887. https://doi.org/10.1039/c3cp52125g.
[41] Z. Hu, Q.N. Liu, S.L. Chou, S.X. Dou, Advances and challenges in metal sulfides/selenides for next-generation rechargeable sodium-ion batteries, Adv. Mater. 29 (2017) 24. https://doi.org/10.1002/adma.201700606.
[42] G. Ali, S.H. Oh, S.Y. Kim, J.Y. Kim, B.W. Cho, K.Y. Chung, An open-framework iron fluoride and reduced graphene oxide nanocomposite as a high-capacity cathode material for Na-ion batteries, J. Mater. Chem. 3 (2015) 10258–10266. https://doi.org/10.1039/c5ta00643k.
[43] D.L. Ma, H.G. Wang, Y. Li, D. Xu, S. Yuan, X.L. Huang, X.B. Zhang, Y. Zhang, In situ generated FeF_3 in homogeneous iron matrix toward high-performance cathode material for sodium-ion batteries, Nano Energy 10 (2014) 295–304. https://doi.org/10.1016/j.nanoen.2014.10.004.

[44] Y.N. Zhou, M. Sina, N. Pereira, X.Q. Yu, G.G. Amatucci, X.Q. Yang, F. Cosandey, K.W. Nam, $FeO_{0.7}F_{1.3}$/C nanocomposite as a high-capacity cathode material for sodium-ion batteries, Adv. Funct. Mater. 25 (2015) 696–703. https://doi.org/10.1002/adfm.201403241.
[45] G.G. Amatucci, N. Pereira, Fluoride based electrode materials for advanced energy storage devices, J. Fluorine Chem. 128 (2007) 243–262. https://doi.org/10.1016/j.jfluchem.2006.11.016.
[46] F. Wang, N. Pereira, G. Amatucci, Y.M. Zhu, J. Graetz, Conversion electrodes for lithium batteries: evolution of nanostructure during lithiation, Abstr. Pap. Am. Chem. Soc. 243 (2012) 1.
[47] F. Badway, N. Pereira, F. Cosandey, G.G. Amatucci, Carbon-metal fluoride nanocomposites - structure and electrochemistry of FeF_3 : C, J. Electrochem. Soc. 150 (2003) A1209–A1218. https://doi.org/10.1149/1.1596162.
[48] A. Goni, L. Lezama, J.L. Pizarro, J. Escobal, M.I. Arriortua, T. Rojo, Intercalation of Cu^{2+} in the $HNiPO_4$ center dot H_2O layered phosphate: study of the structure, spectroscopic, and magnetic properties of the intercalated derivative and the related $CuNi_2(PO_4)_2$ compound, Chem. Mater. 11 (1999) 1752–1759. https://doi.org/10.1021/cm980785w.
[49] J.A. Dean, Lange's Handbook of Chemistry, twelfth ed., McGraw-Hill, New York, New York, 1979.
[50] J. Kim, H. Kim, K. Kang, Conversion-based cathode materials for rechargeable sodium batteries, Ad. Energy Mater. 8 (2018). https://doi.org/10.1002/aenm.201702646.
[51] I. Almodovar, B.C. Frazer, J.J. Hurst, D.E. Cox, P.J. Brown, Magnetic structure of $CuSO_4$, Phys. Rev. 138 (1965). A153-+, https://doi.org/10.1103/PhysRev.138.A153.
[52] Y.G. Wang, Y.R. Wang, E.J. Hosono, K.X. Wang, H.S. Zhou, The design of a $LiFePO_4$/carbon nanocomposite with a core-shell structure and its synthesis by an in situ polymerization restriction method, Angew. Chem. Int. Ed. 47 (2008) 7461–7465. https://doi.org/10.1002/anie.200802539.
[53] X.D. Liu, H.T. Liu, Y.M. Zhao, Y.Z. Dong, Q.H. Fan, Q. Kuang, Synthesis of the carbon-coated nanoparticle Co_9S_8 and its electrochemical performance as an anode material for sodium-ion batteries, Langmuir 32 (2016) 12593–12602. https://doi.org/10.1021/acs.langmuir.6b02870.
[54] H.H. Lyu, B. Gao, F. He, C. Ding, J.C. Tang, J.C. Crittenden, Ball-milled carbon nanomaterials for energy and environmental applications, Acs Sustain. Chem. Eng. 5 (2017) 9568–9585. https://doi.org/10.1021/acssuschemeng.7b02170.
[55] F.X. Wu, G. Yushin, Conversion cathodes for rechargeable lithium and lithium-ion batteries, Energy Environ. Sci. 10 (2017) 435–459. https://doi.org/10.1039/c6ee02326f.
[56] J. Yoshida, E. Guerin, M. Arnault, C. Constantin, B.M. de Boisse, D. Carlier, M. Guignard, C. Delmas, New P2-$Na_{0.70}Mn_{0.60}Ni_{0.30}Co_{0.10}O_2$ layered oxide as electrode material for Na-ion batteries, J. Electrochem. Soc. 161 (2014) A1987–A1991. https://doi.org/10.1149/2.0121414jes.
[57] S.W. Wang, L.J. Wang, Z.Q. Zhu, Z. Hu, Q. Zhao, J. Chen, All organic sodium-ion batteries with $Na_4C_8H_2O_6$, Angew. Chem. Int. Ed. 53 (2014) 5892–5896. https://doi.org/10.1002/anie.201400032.
[58] D. Su, H.J. Ahn, G. Wang, Hydrothermal synthesis of alpha-MnO_2 and beta-MnO_2 nanorods as high capacity cathode materials for sodium ion batteries, J. Mater. Chem. A 1 (2013) 4845–4850. https://doi.org/10.1039/c3ta00031a.
[59] B.M. de Boisse, D. Carlier, M. Guignard, L. Bourgeois, C. Delmas, P2-$Na_xMn_{1/2}Fe_{1/2}O_2$ phase used as positive electrode in Na batteries: structural changes induced by the electrochemical (De)intercalation process, Inorg. Chem. 53 (2014) 11197–11205. https://doi.org/10.1021/ic5017802.
[60] S. Kumakura, Y. Tahara, K. Kubota, K. Chihara, S. Komaba, Sodium and manganese stoichiometry of P2-type $Na_{2/3}MnO_2$, Angew. Chem. Int. Ed. 55 (2016) 12760–12763. https://doi.org/10.1002/anie.201606415.
[61] D.D. Yuan, X.H. Hu, J.F. Qian, F. Pei, F.Y. Wu, R.J. Mao, X.P. Ai, H.X. Yang, Y.L. Cao, P2-type $Na_{0.67}Mn_{0.65}Fe_{0.2}Ni_{0.15}O_2$ cathode material with high-capacity for sodium-ion battery, Electrochim. Acta 116 (2014) 300–305. https://doi.org/10.1016/j.electacta.2013.10.211.
[62] N.B. Mahadi, J.S. Park, J.H. Park, K.Y. Chung, S.Y. Yi, Y.K. Sun, S.T. Myung, Vanadium dioxide - reduced graphene oxide composite as cathode materials for rechargeable Li and Na batteries, J. Power Sources 326 (2016) 522–532. https://doi.org/10.1016/j.jpowsour.2016.07.026.
[63] K. Chihara, N. Chujo, A. Kitajou, S. Okada, Cathode properties of $Na_2C_6O_6$ for sodium-ion batteries, Electrochim. Acta 110 (2013) 240–246. https://doi.org/10.1016/j.electacta.2013.04.100.
[64] R.R. Zhao, L.M. Zhu, Y.L. Cao, X.P. Ai, H.X. Yang, An aniline-nitroaniline copolymer as a high capacity cathode for Na-ion batteries, Electrochem. Commun. 21 (2012) 36–38. https://doi.org/10.1016/j.elecom.2012.05.015.
[65] G. Kresse, J. Furthmuller, Efficiency of ab-initio total energy calculations for metals and semiconductors using a plane-wave basis set, Comput. Mater. Sci. 6 (1996) 15–50. https://doi.org/10.1016/0927-0256(96)00008-0.
[66] P.E. Blochl, Projector augmented-wave method, Phys. Rev. B. 50 (1994) 17953–17979. https://doi.org/10.1103/PhysRevB.50.17953.
[67] J.P. Perdew, K. Burke, M. Ernzerhof, Generalized gradient approximation made simple, Phys. Rev. Lett. 77 (1996) 3865–3868. https://doi.org/10.1103/PhysRevLett.77.3865.
[68] V.I. Anisimov, F. Aryasetiawan, A.I. Lichtenstein, First-principles calculations of the electronic structure and spectra of strongly correlated systems: the LDA+U method, J. Phys. Condens. Matter 9 (1997) 767–808. https://doi.org/10.1088/0953-8984/9/4/002.
[69] A. Jain, S.P. Ong, G. Hautier, W. Chen, W.D. Richards, S. Dacek, S. Cholia, D. Gunter, D. Skinner, G. Ceder, K.A. Persson, Commentary: the Materials Project: a materials genome approach to accelerating materials innovation, Apl. Mater. 1 (2013) 11. https://doi.org/10.1063/1.4812323.